



Open Archive TOULOUSE Archive Ouverte (OATAO)

OATAO is an open access repository that collects the work of Toulouse researchers and makes it freely available over the web where possible.

This is an author-deposited version published in : <http://oatao.univ-toulouse.fr/>
Eprints ID : 19805

To link to this article : DOI : 10.1016/j.ceramint.2016.05.169
URL : <http://dx.doi.org/10.1016/j.ceramint.2016.05.169>

To cite this version : Delon, Elodie and Ansart, Florence and Duluard, Sandrine and Bonino, Jean-Pierre and Malié, A. and Joulia, A. and Gomez, P. *Synthesis of yttria by aqueous sol-gel route to develop anti-CMAS coatings for the protection of EBPVD thermal barriers*. (2016) *Ceramics International*, vol. 42 (n° 12). pp. 13704-13714. ISSN 0272-8842

Any correspondence concerning this service should be sent to the repository administrator: staff-oatao@listes-diff.inp-toulouse.fr

Synthesis of yttria by aqueous sol-gel route to develop anti-CMAS coatings for the protection of EBPVD thermal barriers

E. Delon ^{a,*}, F. Ansart ^a, S. Duluard ^a, J.P. Bonino ^a, A. Malié ^b, A. Joulia ^c, P. Gomez ^d

^a CIRIMAT, Université de Toulouse, CNRS, INPT, UPS, Université Toulouse 3 Paul Sabatier, Bât CIRIMAT, 118 Route de Narbonne, 31062 Toulouse cedex 9, France

^b SNECMA Site de Chatellerault, ZI Nord, rue Maryse Bastié, BP 129, 86101 Chatellerault Cedex, France

^c SAFRAN Tech, Pôle Matériaux et Procédés, rue des Jeunes Bois, Châteaufort, CS 80112, 78772 Magny-Les-Hameaux, France

^d DGA Techniques aéronautiques, 47 rue Saint Jean, 93123, 31131 Balma, France

Anti-CMAS yttria coatings have been prepared by sol-gel routes. Yttria powders with controlled morphology are prepared via auto-combustion of yttrium precursors in a polymerized matrix. The influence of key parameters of the water-based sols is assessed. Indeed, the pH of the initial sol and the temperature of thermal treatment play a major role in the morphology and grain size of yttria powders. To prevent infiltration of CMAS, yttria powders are proposed to be synthesized at pH=1 of the aqueous sol, with drying of the sol and heating at 900 °C. After optimization of the synthesis and deposition conditions via sol-gel route, yttria-based coatings with high specific surface area are obtained. They promote the interaction with melt CMAS and consequently limit the degradation of the thermal barrier coatings situated underneath. It was proved that anti-CMAS yttria coating is effective against the infiltration of CMAS at 1250 °C for 15 min and even 1 h.

1. Introduction

Thermal barrier coatings systems (TBCs) are widely used to protect critical metallic parts of gas turbine engines as blades, vanes, seals and combustion chambers because of their excellent thermal protection properties [1,2]. TBCs are multilayered systems including: (i) the TBC itself, a thermal insulating porous ceramic top coat, generally composed of 8 wt% yttria partially stabilized zirconia (YSZ), (ii) an aluminum rich bond coat which improves the cohesion between the metallic substrate and the TBC, (iii) a thin alumina film called thermally grown oxide (TGO), and (iv) the nickel-based superalloy that supports mechanical loading. For turbine blades, the ceramic coating is industrially deposited by electron beam physical vapor deposition (EB-PVD). In this case, the coating exhibits a porous columnar microstructure resulting in a moderately low thermal conductivity and a quite high strain tolerance.

Nowadays, despite the improvement of the engine efficiency, TBCs in service are prone to intrinsic and extrinsic degradation phenomena which may considerably restrict their durability. At higher and higher temperatures and under specific service conditions, TBCs are exposed to degradation by molten calcium-

magnesium-alumino-silicates, commonly called CMAS, resulting from the ingestion by the engine of mineral debris as ash, dust, sand, ..., contained in the hot gases entering the turbine [3,4]. This attack mainly induces two types of degradation mechanisms in the TBCs. First as the temperature of TBC surface is higher than the melting temperature of the CMAS, these deposits form low viscosity glassy melts which infiltrate the porous columnar microstructure of the TBC. Upon cooling, the infiltrated TBC becomes rigid resulting in the loss of strain tolerance and activated failure of the TBC. Delamination cracks can develop themselves in the top coat leading to progressive spallation during thermal cycling. This phenomenon is similar to a heat shock. The second mechanism is related to the chemical interaction between molten CMAS and YSZ. YSZ is dissolved into the molten CMAS and, upon saturation, a new crystalline phase at the interface CMAS/YSZ precipitates. This phenomenon deteriorates the columnar porous morphology. These thermomechanical and thermochemical degradations are the most detrimental for the TBC [5–7], indeed, the superalloy is no longer protected.

In the literature, different types of coatings: non-wetting, sacrificial or impermeable coatings, are proposed to prevent degradation of TBCs [8–10]. The non-wetting coatings reduce the contact between the CMAS melts and the ceramics layers. The impermeable coatings inhibit the infiltration of the melt CMAS. The sacrificial coatings react with the CMAS to increase its melting temperature or its viscosity to prevent their infiltration into the

* Corresponding author.

E-mail address: delon@chimie.ups-tlse.fr (E. Delon).

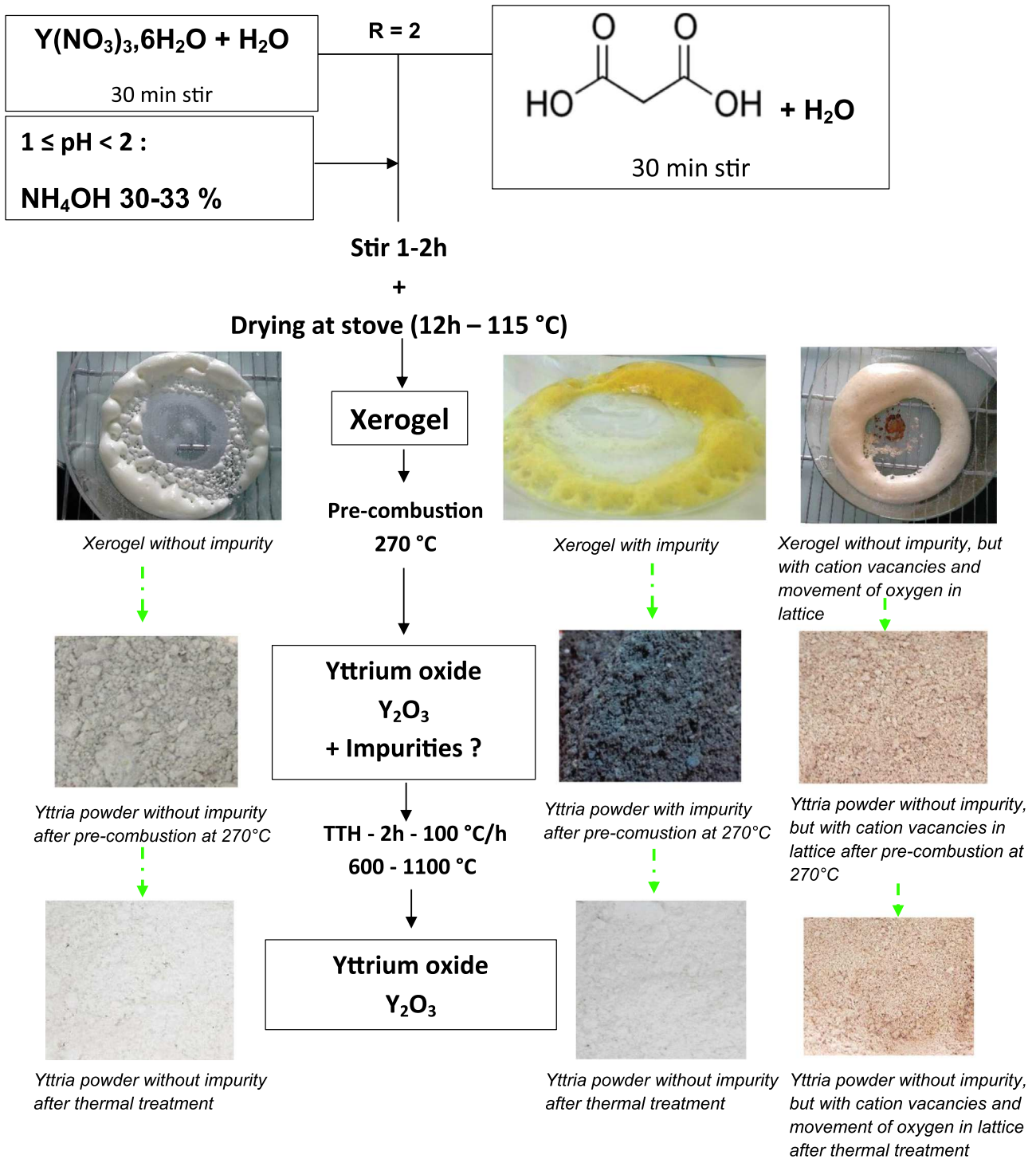


Fig. 1. Protocol of yttria synthesis.

thermal barrier. The compositions of such sacrificial coatings usually used are: SiO_2 , Al_2O_3 , Sc_2O_3 , Cr_2O_3 , MgO , CaO , alumina particles incorporated into a silica matrix, $\text{Gd}_2\text{Zr}_2\text{O}_7$, Nd_2O_3 , $\text{Nd}_2\text{Zr}_2\text{O}_7$, Y_2O_3 or yttria stabilized zirconia [9].

Some preliminary investigations carried out in our research group [10], show that yttria coatings are a good solution to protect thermal barrier coatings from these contaminants and precisely to prevent their infiltration. Nevertheless, in these previous works, the microstructure was not optimized even if the yttria compound has a very high reactivity with molten CMAS resulting in the rapid precipitation of complex oxides. Relative to the

mechanism, yttria can be seen as a Y^{3+} reservoir, and after its dissolution, it allows the formation of the apatite crystalline phase $\text{Ca}_4\text{Y}_6\text{O}(\text{SiO}_4)_6$. The cation Y^{3+} is really efficient to stop the infiltration of CMAS because it reacts almost instantly, from about 1200 °C, with silicates to form the apatite phase $\text{Ca}_4\text{Y}_6\text{O}(\text{SiO}_4)_6$ which solidifies and inhibits infiltration. Moreover, the calcium and silicon from the molten glass are consumed, leading to a local chemical modification of the silicate and to the crystallization of the CMAS. This phenomenon causes the annihilation of the effects due to CMAS and can limit damage of the thermal barrier system.

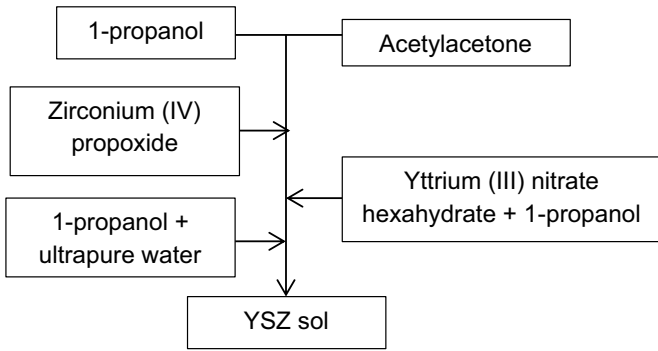


Fig. 2. Protocol of YSZ sol.

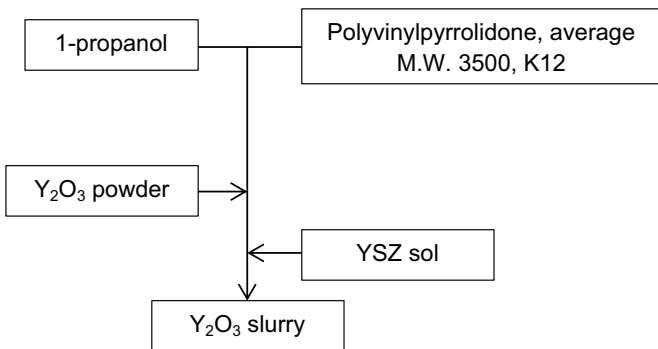


Fig. 3. Protocol of yttria slurry preparation.

Of course, the yttria coating must present a good compromise in terms of density: a sufficient low porosity to avoid direct CMAS infiltration, but not completely dense to avoid cracks and to accommodate thermomechanical stresses. Moreover, the leveling at the ceramic surface is preferred in order to allow a good adaptation of the thermomechanical stresses during cyclic oxidation.

The synthesis of yttria can be performed by many routes [11–13]. Dupont et al. [14,15], via the sol-gel route, prepare yttria nanopowders from citric acid, tartaric acid, acid malonic and ethanoic acid by both chelation and/or polymerization. The ratio [chelating agent]/[Y] and the heat treatment temperature (800 °C or 1100 °C), mainly influence the particles morphology.

Yttria is then deposited onto an EB-PVD thermal barrier by dip-coating via the alkoxide sol-gel process. The sol-gel method is a versatile and innovative process resulting from the wet route which allows to synthesize a wide variety of materials of high purity at relatively low temperatures and even at room temperature, in water or organic solvents and in a wide range of pH or ionic strength conditions. There are two sol-gel synthesis routes: i) inorganic or colloidal route obtained from metal salts (chlorides, nitrates ...) in aqueous solution; and ii) organometallic or polymeric way obtained from metal alkoxides on organic solutions. By this kind of route, it is easier to control the homogeneity, stoichiometry, crystalline structure and size of the synthesized

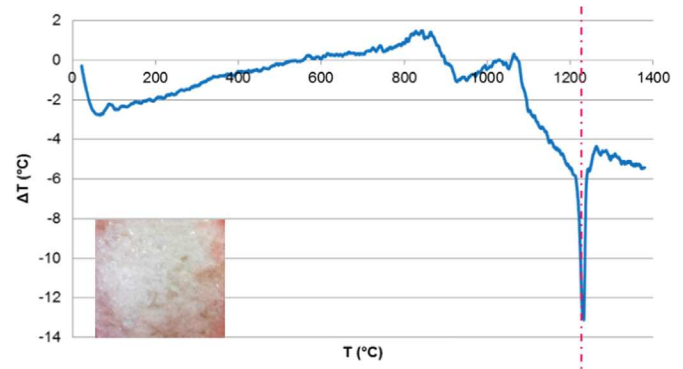


Fig. 5. DTA of CMAS.

compounds. The ease of implementation of this technique allows the development of multilayer coatings, multi-material, gradient composition ... with strict control of chemical composition, which can be made on complex parts with a lower cost than industrial processes currently used. In our study, yttria is synthesized via inorganic or colloidal sol-gel and deposited by dip-coating on EB-PVD systems to functionalize and confer them additional anti-CMAS properties.

The main aim of this paper is to define the optimized “morphology” of powder to be shaped into efficient anti-CMAS coatings. So, we propose to investigate the influence of different parameters such as the pH of the initial sol and the temperature of thermal treatment consecutive to the auto-combustion treatment on the morphology and size of yttria particles. These particles will enter the formulation of loaded alkoxide sols to prepare yttria-based anti-CMAS coatings. Finally, to evaluate the efficiency of the protected coating, a “reference” CMAS [33.2CaO–6.5MgO–11.9 Al₂O₃–48.5 SiO₂ wt%] has been synthesized. This CMAS has a composition similar to that commonly used in the literature [6,7] and is representative of the average chemical composition of CMAS found on real parts [16]. The interaction between this CMAS composition and yttria coating has been studied and compared to non-coated EB-PVD thermal barrier.

2. Material and methods

2.1. Synthesis of yttria powders

The synthesis of yttria powder is based on the protocol established by Dupont [14,15]. The chelating agent used is malonic acid. The [malonic acid]/[Y] ratio used is 2. Fig. 1 shows the synthesis protocol of yttria sol-gel. To synthesize yttria, hexahydrate yttrium (III) nitrate solution Y(NO₃)₃·6H₂O (Sigma-Aldrich, C=0.5 M), malonic acid solution CH₂(COOH)₂ (Sigma-Aldrich, C=2 M) and ultrapure water are used as raw precursors. The yttrium atom is chelated by several molecules of malonic acid to complete its coordination sphere. The units are linked together by hydrogen

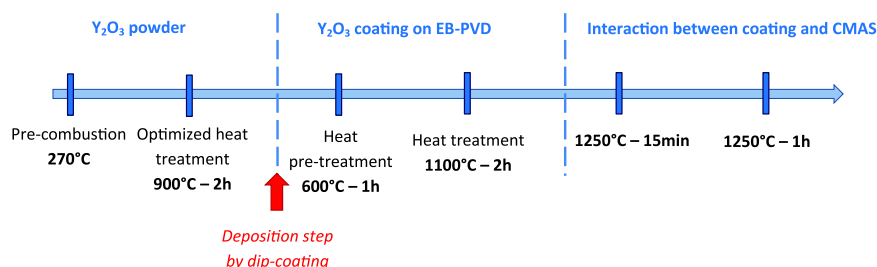


Fig. 4. Global scheme of protocol: optimized process.

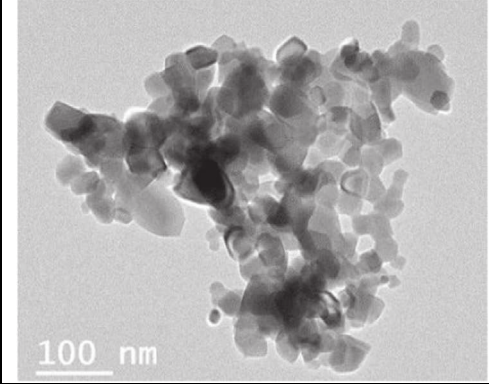
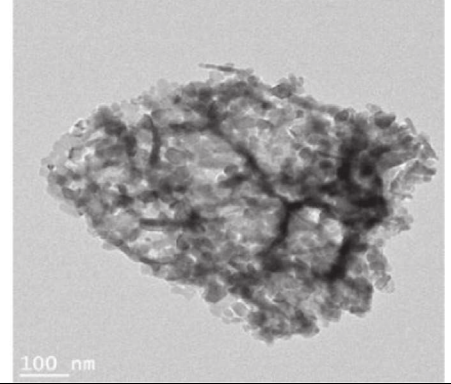
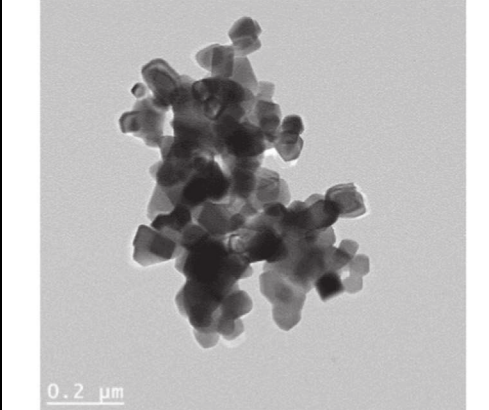
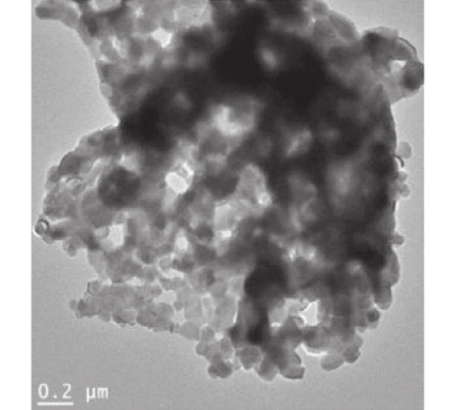
T (°C) \ pH	a) 25000x	1	b) 25000x	1.7
900				
		$\varnothing_{\text{average particle}} \approx 60 \text{ nm}$		$\varnothing_{\text{average particle}} \approx 40 \text{ nm}$
1100				
	c) 20000x	$\varnothing_{\text{average particle}} \approx 80 \text{ nm}$	d) 10000x	$\varnothing_{\text{average particle}} \approx 70 \text{ nm}$

Fig. 6. Influence of pH on yttria sol – TEM analysis – a) 25,000 ×, T=900 °C, pH=1; b) 25,000 ×, T=900 °C, pH=1.7; c) 20,000 ×, T=1100 °C, pH=1; d) 10,000 ×, T=1100 °C, pH=1.7.

Table 1
Specific surface area S_w of yttria as a function of pH and temperature.

T (°C)	600	700	800	900	1000	1100
pH=1	45.1 ± 0.1	36.1 ± 0.3	30.1 ± 0.1	17.8 ± 0.2	13.8 ± 0.1	9.3 ± 0.1
pH=1.7	20.3 ± 0.1	12.0 ± 0.1	10.5 ± 0.1	9.9 ± 0.1	8.2 ± 0.1	6.6 ± 0.1

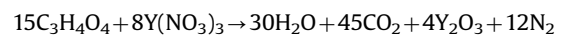
Table 2
Pore volume of yttria as a function of pH and temperature.

T (°C)	600	700	800	900	1000	1100
pH=1	261.4	237.2	187.4	127.8	100.7	59.7
pH=1.7	147.6	121.0	81.0	65.7	64.3	52.3

bonds maintaining stability of the structure. Drying at the stove reduces the volume of water. Molecules move and associate through hydrogen bonds. This implies a short range order. No regular extended entity is formed. Only reducing the amount of water that occurs, water retention by the precursor can be noticed and a gel is obtained. The pH can be adjusted by addition of ammonium hydroxide NH_4OH (Sigma-Aldrich) at 30–33%. In fact, at a pH less than 1, the gel does not form and above pH=2, yttrium hydroxide forms a white precipitate. Several pH values were investigated to evaluate the effect on yttria particle morphology. Two intermediate pH values for the sol have been chosen for the

study: pH=1 and 1.7. Then they evolve during the 12 h of heating at 115 °C in a stove. After the drying, the gel is pearly or yellow.

The chemical reaction involving the various reagents to prepare yttria, is the following:



In these synthesis conditions ([malonic acid]/[Y] ratio equal to 2), a spontaneous self-combustion was observed at 270 °C [14]. So the gel is then placed in a combustion furnace at 270 °C to generate the self-combustion. This step is called pre-combustion. The formation of the gel, removal of organic compounds and the exothermicity of the reaction are sufficient to initiate a self-combustion phenomenon leading to the formation of an ultra-porous material similar to a foam. Yttria powder can be white if it has no impurity or black if organic materials are still present after pre-combustion at 270 °C. In this case, the reaction was not complete probably because of a lack of oxidant agent (nitrate). The yttria is then manually crushed in a mortar after combustion in order to

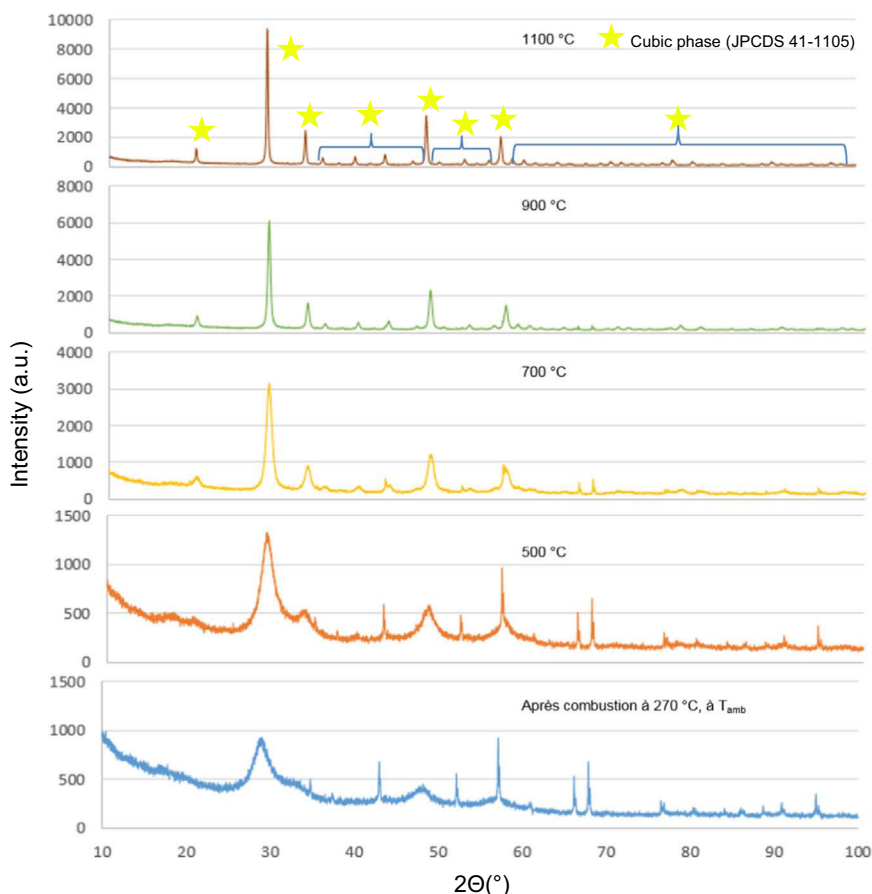


Fig. 7. Temperature XRD of yttria after pre-combustion at room temperature to 1100 °C.

Table 3
Crystallite size calculated by Scherrer technique.

T (°C)	After combustion, T _{amb}	600	700	800	900	1000	1100
D (nm)	< 5	≈ 8	≈ 10	≈ 15	≈ 20	≈ 30	≈ 40
Accuracy	< 5						
10%							

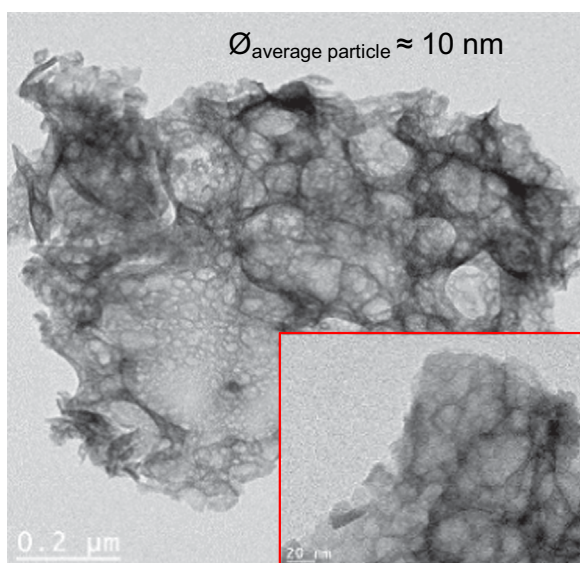


Fig. 8. Influence of temperature on yttria – TEM analysis: at pH=1 and T=270 °C before heat treatment – 20,000 ×, 100,000 ×.

reduce the size of aggregates. To synthesize yttria powder without impurities to remove organic materials due to the synthesis present even after pre-combustion at 270 °C, a heat treatment of 2 h was performed after pre-combustion in a furnace under air. Several heat treatment temperatures were investigated on yttria powder from 600 °C to 1100 °C (up/down ramps: 100 °C/h) in order to study the influence of this parameter on the morphology and particle size of yttria. After the optimized heat treatment, the yttria powder is “pure”, without impurity. It is possible to obtain beige yttria powders, this coloration phenomenon is due to the cation vacancies and the movement of oxygen in the crystal lattice of yttria. However, the synthesized fine powder is suitable to be used.

2.2. Preparation of yttria coatings

An yttria stabilized zirconia (YSZ) sol is made from zirconium (IV) propoxide (Sigma-Aldrich) and yttrium (III) nitrate hexahydrate (Sigma-Aldrich) (Fig. 2). After thermal treatment (600–1100 °C), yttria powders, are incorporated into the slurry made of 1-propanol and YSZ sol (Fig. 3). Yttria based slurries are deposited by dip-coating technique with a Nima Technology Micro-Processor Interface IU4 device dip-coater, onto EB-PVD thermal barriers. EB-PVD samples provided by Safran group are 100–200 μm thick and made of YSZ with 6–10 wt% Y₂O₃, the supported alloy being nickel-based superalloy. The experiments are carried out controlling the withdrawal speed of dip-coating (at 250 mm/min) in a chamber with both controlled temperature at room temperature and humidity rate between 60% and 80%. Several immersions are performed in order to reach the suitable layer thickness (around 50–100 μm). In order to favor the anchorage of this top layer, a pre-

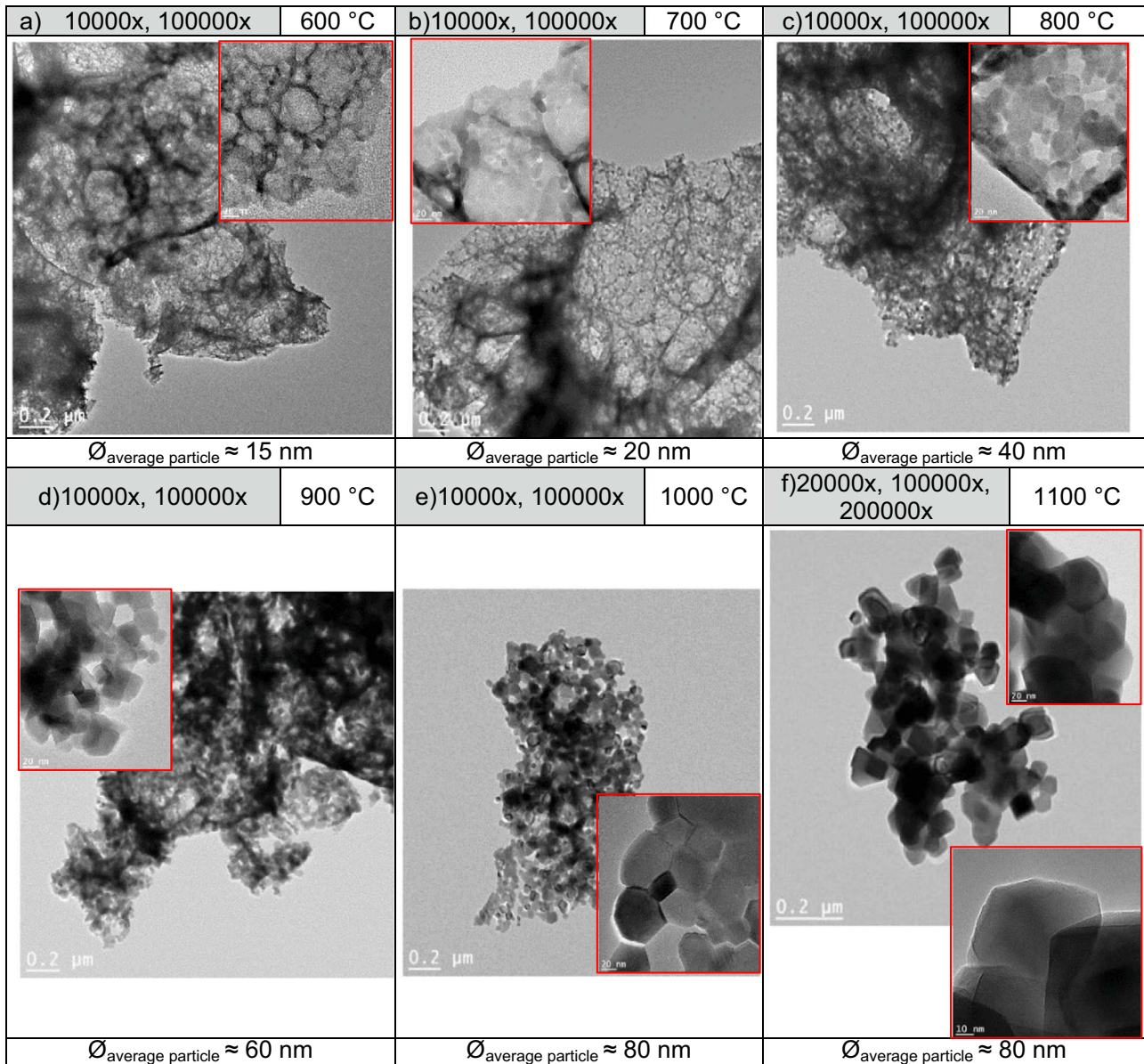


Fig. 9. Influence of temperature on yttria at pH=1 – TEM analysis – a) 10,000 ×, 100,000 ×, 600 °C; b) 10,000 ×, 100,000 ×, 700 °C; c) 10,000 ×, 100,000 ×, 800 °C; d) 10,000 ×, 100,000 ×, 900 °C; e) 10,000 ×, 100,000 ×, 1000 °C; f) 20,000 ×, 100,000 ×, 200,000 ×, 1100 °C.

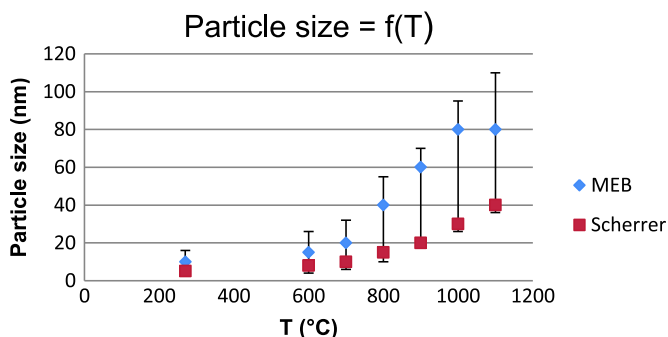


Fig. 10. Influence of temperature on particle and crystallite sizes.

bonding layer is first deposited onto the EB-PVD thermal barrier from an yttria stabilized zirconia sol. Finally, after complete deposition, a first heat pre-treatment at 600 °C for 1 h is realized on the coating to remove organic materials due to the residues of YSZ sol, then a second treatment at 1100 °C for 2 h in air (up/down

ramp:50 °C/h) is carried out on the coating to sinter it and to obtain a good stress resistance, indeed under oxidation cycling conditions, coating is tested at 1100 °C.

A scheme of the global protocol is represented in Fig. 4.

2.3. Synthesis of CMAS compounds and chemical interaction with yttria coating

A “reference” CMAS composition corresponding to the more classically reported in literature [6,7] is then synthesized from simple CaO calcium oxide (Aldrich, purity 99%), MgO magnesium oxide (Sigma-Aldrich, purity ≥ 99%), Al₂O₃ aluminum oxide (Sigma-Aldrich, purity ≥ 99.9%) and SiO₂ silicon oxide (Sigma-Aldrich, purity ≥ 99.9%) mixed with ultra-pure water (stir for 30 min) to minimize impurities. The composition of this “reference” CMAS is as follows: 33.2CaO–6.5MgO–11.9Al₂O₃–48.5 SiO₂ wt%. The raw materials are placed in a stove at 80 °C for at least 12 h before manual grinding. Then, they are put into a platinum crucible and placed in a preheated furnace at 1400 °C for 1 h followed by

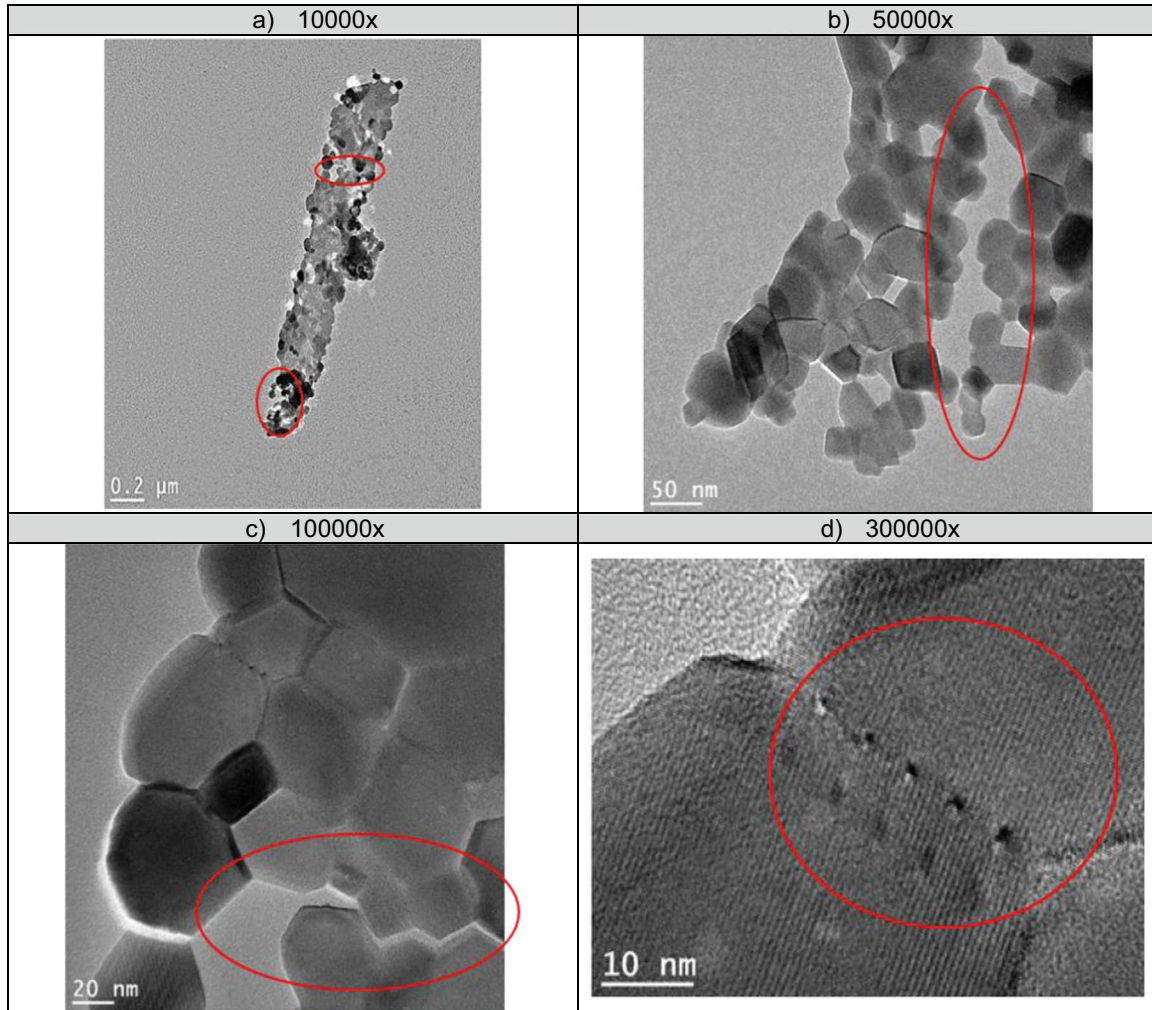


Fig. 11. Phenomenon of deagglomeration – TEM analysis: at pH=1 and T=1000 °C – a) 10,000 ×; b) 50,000 ×; c) 100,000 ×; d) 300,000 ×.

quenching in water to obtain a glassy material. They are then manually crushed in a mortar. The melting temperature is determined by DTA analysis in Fig. 5 in the range [1225–1235 °C]. Compared to the literature [10], the melting temperature must be in the range [1235–1240 °C] but in our case, reactivity is a little more important. To check the effectiveness of our sacrificial coating of yttria, CMAS is deposited onto yttria coating, after heat treatment of coating (600 °C-1 h, 1100 °C-2 h), with a contamination rate of 10 mg/cm². The coatings are placed during 15 min and 1 h in a preheated furnace at 1250 °C, this heat treatment is followed by a quenching in air.

2.4. Characterization techniques

Differential Thermal Analysis (DTA) analyses on SETARAM 92-16.18 TGA92 device were realized under purge air from room temperature at 1400 °C with a speed of 10 °C/min. Transmission Electron Microscopy (TEM) analyses, using a JEOL JEM 2100F-EDS device, were performed to study the morphology and microstructure of yttria powders. The X-Ray Diffraction (XRD) analyzes of these powders were made on the DRX D4 ENDEAVOR 758 Bruker AXS and D8 ADVANCE 205,536 Bruker devices (2 θ interval between 10° and 100°, step of 0.016° and 23 s by step, copper radiation $K_{\alpha 1}=0.15406$ nm, $K_{\alpha 2}=0.15444$ nm). Brunauer-Emmett-Teller theory (BET) analyses were performed on the apparatus Micromeritics Tristar II and Smart VacPrep Micromeritics with degassing at 90 °C for 2 h and heat treatment 200 °C for 10 h. The

coating thickness was first controlled from Fisher Dualscope FMP20 device and then by Scanning Electron Microscope (SEM) JSM 6510 LV and Field Emission Gun (FEG) – Scanning Electron Microscope (SEM) JEOL JSM 7800F Prime EDS. Energy Dispersive X-ray Spectrometry (EDS) analyses were carried out with the FEG-SEM JEOL JSM 7800F Prime EDS to study the interactions yttria/CMAS.

3. Results and discussion

3.1. Synthesis of yttria powders

3.1.1. Influence of pH on the morphology and microstructure at a given temperature

Fig. 6 shows the influence of pH on the morphology of yttria powders synthesized at 900 °C, in Fig. 6(a) and (c) and 1100 °C in Fig. 6(b) and (d). For the powder prepared at pH=1.7, the microstructure is aerated, the agglomerates obtained are similar to a foam with rather spherical particles. These particles form bridges and maintain the foam. In contrast, at pH=1, the morphology of the agglomerates seems to be denser and foam-like shapes supported by the particles are not observed. The bridges are broken. In addition, the particles are not spherical but cubic. The particles made at pH=1 (at 900 °C, approximately 60 nm) are about two times larger than those produced at pH=1.7 (at 900 °C, approximately 40 nm) due to a quite different reaction progress.

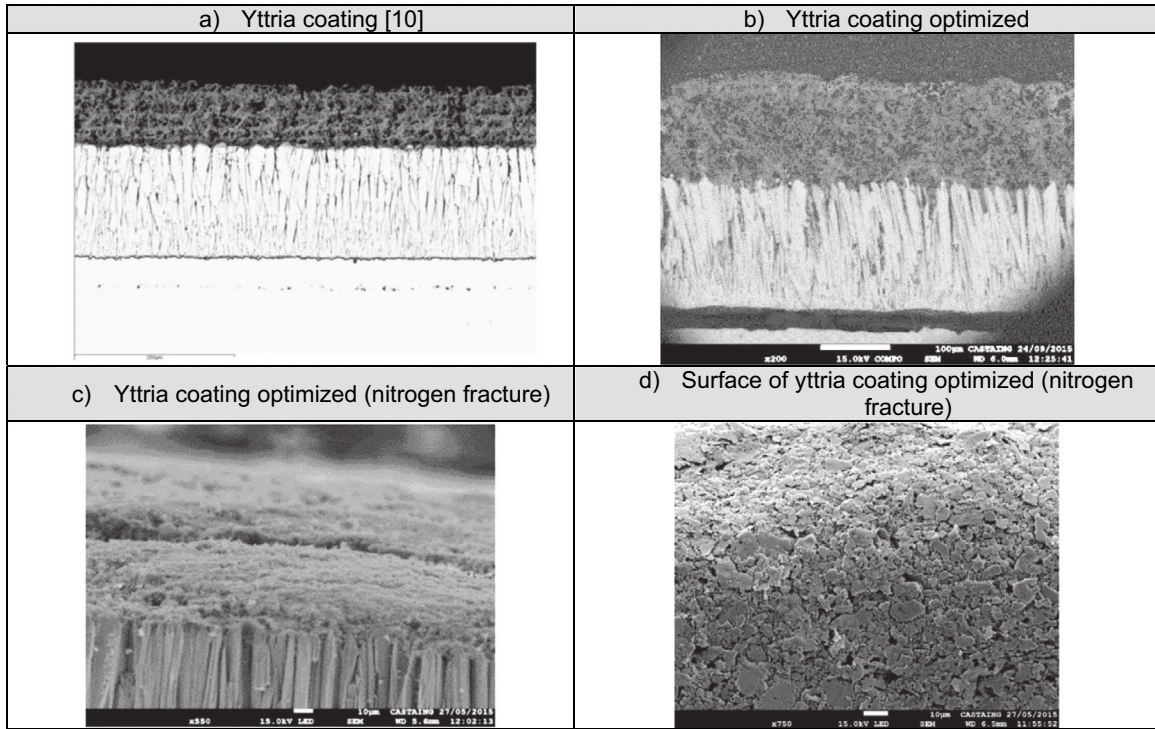


Fig. 12. Yttria coating – FEG-SEM analysis – a) Yttria coating [10]; b) Yttria coating optimized; c) Yttria coating optimized (nitrogen fracture); d) Surface of yttria coating (nitrogen fracture).

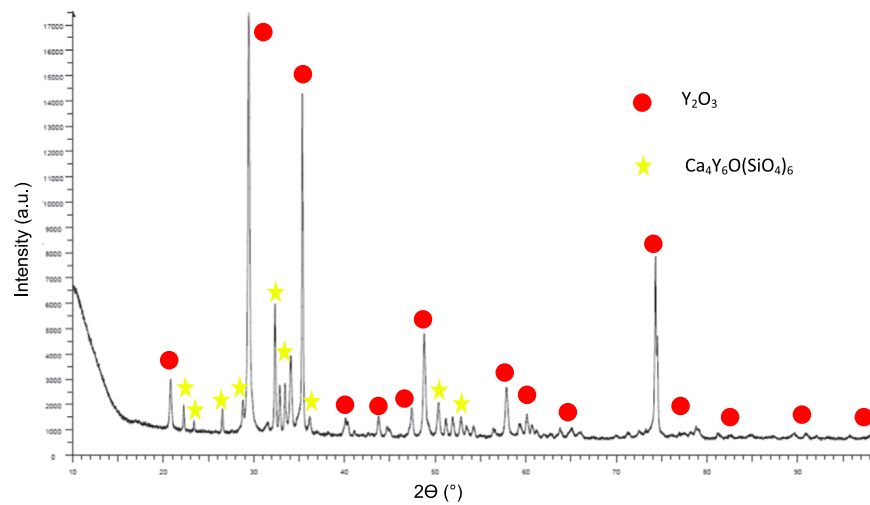


Fig. 13. XRD analysis – Interaction between yttria coating and CMAS.

Tables 1 and 2 show BET analyses conducted on yttria powders synthesized at different pH values and heat treatment temperatures to determine their influence on the specific surface area and the pore volume.

Whatever the pH, the specific surface areas and the total pore volumes decrease when the heat treatment temperature increases. But, for pH=1, the specific surface and the pore volume are larger than for pH=1.7. This is well correlated with the TEM observations discussed above, with larger agglomerates for the particles synthesized at pH=1.7. Nevertheless, on the observations by TEM (Fig. 6), the particles synthesized at pH=1 have a larger size (mean size of 60 nm compared to 40 nm for pH=1.7 at 900 °C) but are well individualized. For pH=1.7, particles are smaller but interconnected and agglomerated which induces a decrease in the evolution of specific surface area. If we compare now the values of the specific surface areas (S_w) and pore volumes at the two pH

values, we note that from 600 °C to 1100 °C, the values obtained at low pH have more drastic decrease (45.1–9.3) compared to those obtained for a higher pH (20.3–6.7). But if we consider the S_w value at 1100 °C, we notice a slight higher value (9.3 compared to 6.7 for pH=1 and pH=1.7 respectively) so this family of powder corresponding to pH=1 is expected to be more suitable for the next shaping step.

To summarize the step of the synthesis of yttrium oxide, the pH has a major influence on the morphology of the yttrium oxide. Several studies have already pointed out the influence of pH on the morphology, size, and particle properties in the case of the sol-gel route. The BET and TEM analyses, performed in our study, show that the particles synthesized at pH=1 have a larger specific surface area whatever the temperature than for pH=1.7. This phenomenon can be explained by the DLVO theory [17–19], at low pH, the electrical layer of the particles is destroyed causing significant

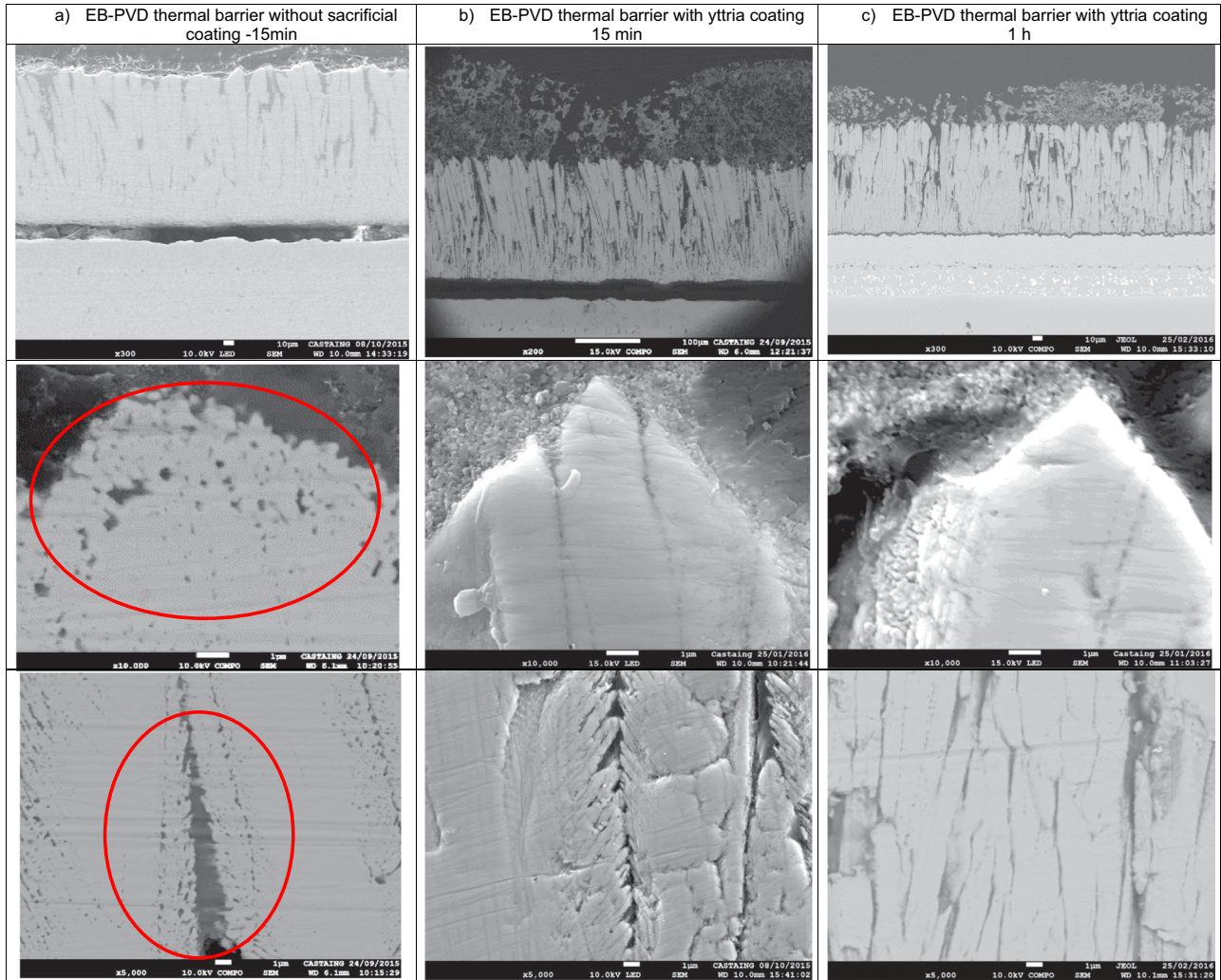


Fig. 14. Interaction between CMAS and EB-PVD thermal barrier without/with yttria coating for 15 min and 1 h at 1250 °C – FEG-SEM analysis– Global view of coating, view of the top of the columns of EB-PVD, view of the middle of the columns of EB-PVD – a) EB-PVD thermal barrier without sacrificial coating – 15 min; b) EB-PVD thermal barrier with yttria coating – 15 min; c) EB-PVD thermal barrier with yttria coating – 1 h.

aggregation of particles between them. Indeed, the stability of a suspension is governed by DLVO theory that considers the total potential of interaction between two particles is the sum of the attractive and repulsive potentials, and the pH plays a significant role in this potential. The pH influences the crystallite size and specific surface area. At $\text{pH}=1.7$, the electric layer including the particles is always present which prevents aggregation.

So with the aim to densify the anti-CMAS coating, it is better to choose yttria powders synthesized at $\text{pH}=1$.

3.1.2. Influence of temperature on the morphology and microstructure

As shown by XRD analyses, yttria powders exhibit a cubic crystalline structure (file JPCDS 41-1105) with the lattice parameter $a=10.604 \text{ \AA} \pm 0.001 \text{ \AA}$ whatever the pH, after drying or heat treatment. This cubic nature is more or less marked after combustion depending on the purity of the synthesized powder. It is important to underline that in Fig. 7, higher the temperature, narrower the diffraction peaks from room temperature to 1100 °C showing a progressive crystal growth. This is confirmed by the values of the crystallite size calculated by the Scherrer technique in Table 3.

TEM analyses show that the temperature influences the particle morphology before heat treatment in Fig. 8 (particle size after

pre-combustion at 270 °C: around 10 nm) and after heat treatment (from 600 °C at 1100 °C) in Fig. 9 (particle size at 1100 °C: around 80 nm). When the temperature increases, the foam morphology tends to disappear. Indeed, after pre-combustion, the morphology is very aerated, the spherical particles maintain the foam structure by bridges (Fig. 9(a)–(c)). When the temperature increases from 600 °C at 1100 °C, the bridges break themselves and the foam collapses (Fig. 9(d)–(f)), the agglomerates size decreases (around 5 μm at 600 °C, less than 1 μm at 1100 °C). In fact, crystallite size highly exceeds the dimension of the particle and the breakage of the crystallites is between them (Fig. 9(d)). The particles merge, grow (size increases by a factor of about 10–1100 °C) (Fig. 10) and their reactivity decreases. This is a classical behavior reported in literature [20–22]. Indeed, increasing the heat treatment temperature, small particles coalesce in favor of bigger, there is diffusion. This process is realized because it is less expensive in terms of surface energy to have a single large particle compared to two small ones. It is confirmed by TEM patterns and BET analyses. When temperature increases, changes on the geometric parameters may be identified by the appearance of facets in the plane of grain boundary, by a simple dissociation or by a rough transition [23]. Indeed, in parallel, the crystallization of the powder takes place, the particles are then faceted at high temperature and cubic shape in Fig. 9(f). Their surface energy is minimized by their cubic shape.

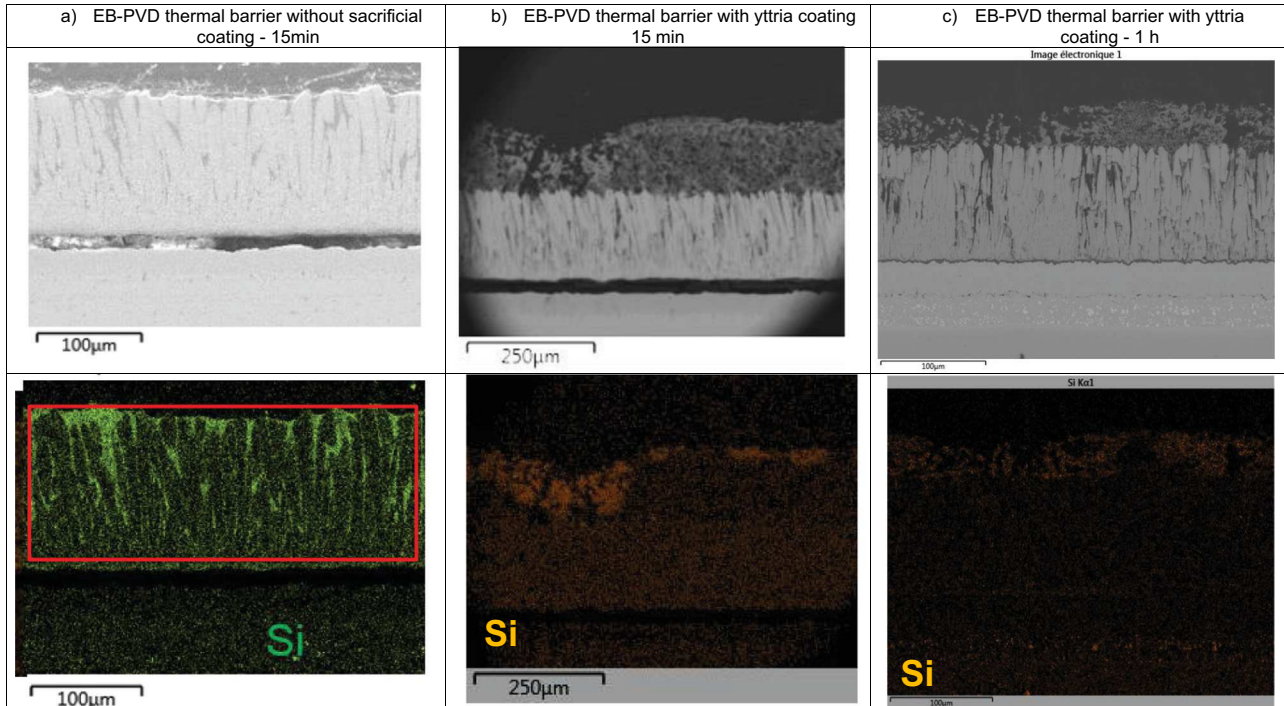


Fig. 15. Interaction between CMAS and EB-PVD thermal barrier without/with yttria coating for 15 min and 1 h at 1250 °C – EDS analysis: K_{α} (Si) – a) EB-PVD thermal barrier without sacrificial coating – 15 min; b) EB-PVD thermal barrier with yttria coating – 15 min; c) EB-PVD thermal barrier with yttria coating – 1 h.

The evolution of the size of the crystallites results in a widening of the grain boundaries with an angle equal to 125°, characteristic of oxides. Indeed the surface forces are balanced (Fig. 9(c)–(f)). The energy supplied by a heating at high temperature leads to sufficient growth to this characteristic dimension.

An interesting point is also to focus at a temperature of 1000 °C (Fig. 11). At this temperature, we can notice by TEM shaped crystallites with bridges between them and well-defined grain boundaries at different magnitudes. So a temperature between 900 °C and 1000 °C seems to be a threshold temperature between different various behaviors: i) below 900 °C, particles have not sharp borders and the crystallization process has just begun, agglomerated particles have a foam structure with spherical particles; ii) at 900 °C, the foam structure tends to disappear and particles morphology becomes cubic. In this case, yttria powder is more reactive than yttria powder heat treated above 900 °C, the porosity of agglomerates is reduced; iii) above 900 °C, crystallites are well identified and separated and their size increases with the heat treatment temperature.

Relative to the particle size, we have reported a graph (Fig. 10) corresponding to the calculated values from Scherrer (Table 3) and we have added on it the range of particles size (determined from MET observations) for each temperature. We can check that we are, in all cases, in the same order of magnitude and we can conclude that we mainly have monocrystalline particles or particles consisted of 2 or 3 crystallites.

In order to reach a compromise between reactivity and convenient microstructure to reduce the porosity of the coating, yttria powder will be synthesized, after a drying step, at pH=1 and heat-treated at 900 °C. Then, the yttria coating is heated at 1100 °C. The decreasing of temperature from 1100 °C (temperature of heat treatment of coating) to 900 °C (temperature of heat treatment of powder) allows to preserve an energy gap in order to promote the establishment of links and a better mechanical anchorage between the powder and the matrix of the coating during the final heat treatment. Previous studies [10] have clearly shown that a temperature gap of 200 °C=1100–900 °C is good enough to have a convenient toughness at the interface.

3.2. Preparation and study of the behavior of yttria coating against CMAS contamination

3.2.1. Preparation of yttria coatings

Yttria coating is then deposited on the EB-PVD thermal barrier by dip coating in Fig. 12. The sacrificial yttria coating covering the EB-PVD thermal barrier, presents a homogeneous appearance and no apparent cracking. This coating is between 50 and 100 µm thick. It is leveling and has a non-oriented microstructure with low porosity. Compared to previous studies [10], the porosity of the coating was reduced.

3.2.2. Chemical interaction with yttria coating

CMAS at a concentration of 10 mg/cm² is brought at the surface of yttria coating and then heat treated for 15 min and 1 h at 1250 °C. The XRD analyses in Fig. 13 indicate that the Ca₄Y₆O (SiO₄)₆ apatite phase is formed on the surface during the interaction. We compared, under the same conditions of interaction, these thermal barriers and a thermal barrier without sacrificial coating in Fig. 14. In the case of unprotected thermal barrier, FEG-SEM analyses in Fig. 14(a) shows that the infiltration is observed on the whole thickness of the barrier, which is confirmed by EDS analyses in Fig. 15(a). Indeed, the thermal barrier is strongly attacked at the top of the columns and in the inter-columnar spaces. According to the literature [5–7], this infiltration causes phase changes in the thermal barrier, in particular with yttrium depletion leading to the transformation of the metastable tetragonal phase into the monoclinic phase. This transformation induces significant volume changes during cooling causing delamination of the thermal barrier. However, when the thermal barrier is protected by yttria coatings, FEG-SEM and EDS analyses respectively in Fig. 14(b) and (c) and in Fig. 15(b) and (c) show that there is no infiltration for 15 min and 1 h at 1250 °C. The microstructure of the top of the columns and feathers is well preserved. The CMAS infiltration is quenched by the sacrificial coating of yttria. CMAS is especially present in the top coating of yttria, it has interacted with it to form new phases and to limit the infiltration. The EB-

PVD thermal barrier is free of CMAS.

So yttrium has an important influence on the limitation of CMAS degradation. Indeed, some studies have shown that the cation Y^{3+} is effective to stop the infiltration of CMAS because it almost instantly reacts with silicates to form the $Ca_4Y_6O(SiO_4)_6$ apatite phase inhibiting infiltration [9,10]. The yttria compound exhibits a very high reactivity with the melt CMAS, this results in the rapid formation of precipitates of complex oxides.

The yttria compound partially dissolves and allows the formation of the apatite phase. Therefore, it serves as yttrium reservoir causing the annihilation of the effects due to CMAS and limiting damage to the thermal barriers. This causes the calcium and silicon consumption from the molten glass, leading to a local chemical modification of the silicate and the crystallization of CMAS.

4. Conclusion

We developed a sacrificial coating to limit the damage caused by the infiltration of CMAS in thermal barriers. The sol-gel method was used to synthesize the coatings. This process is innovative and allows the development of nanostructured materials. The sacrificial coating was developed from yttria layer. The yttria, yttrium reservoir, traps CMAS forming the apatite phase. We studied its synthesis to optimize the coating by densifying the material in order to obtain a barrier to CMAS. These parameters are the pH and the heat treatment temperature. They influence the size, the morphology and microstructure of yttria obtained. Thus, yttria powder is synthesized at pH=1 and with a heat treatment temperature equal to 900 °C. The yttria was then deposited by dip-coating, dipping technique, on the EB-PVD thermal barrier. To test the effectiveness of the coating, interactions with CMAS reference were performed. We are able to achieve an anti-CMAS coating of yttria dense enough to limit the infiltration of CMAS into EB-PVD thermal barrier. This coating has proven efficiency against the infiltration of CMAS at high temperature for a limited time (15 min and 1 h at 1250 °C). Even if these conditions correspond to a severe attack, other tests will be performed to test in parallel the yttria coating in several working conditions.

Acknowledgments

The authors gratefully acknowledge the SAFRAN group for thermal barrier coatings samples and the French Defence Research Organization (DGA) (DGA Grant n° 2014.60.0057) and SAFRAN Tech for the financial support.

References

- [1] M. Peters, C. Leyens, U. Schulz, W.A. Kaysser, EB-PVD thermal barrier coatings for aeroengines and gas turbines, *Adv. Eng. Mater.* 3 (4) (2001) 193–204.
- [2] U. Schulz, C. Leyens, K. Fristscher, M. Peters, B. Saruhan-Brings, O. Lavigne, J. M. Dorvaux, M. Poulain, R. Mervel, M. Caliez, Some recent trends in research and technology of advanced thermal barrier coatings, *Aerosp. Sci. Technol.* 7 (2003) 73–80.
- [3] C. Mercer, S. Faulhaber, A.G. Evans, R. Darolia, A delamination mechanism for TBC subject to CMAS infiltration, *Acta Mater.* 53 (2005) 1029–1039.
- [4] H. Peng, L. Wang, L. Guo, W. Miao, H. Guo, S. Gong, Degradation of EB-PVD TBC caused by CMAS deposits, *Mater. Int.* 22 (5) (2012) 461–467.
- [5] M.H. Vidal-Setif, N. Chellah, C. Rio, C. Sanchez, O. Lavigne, Calcium-magnesium-alumino-silicate (CMAS) degradation of EB-PVD thermal barrier coatings: characterization of CMAS damage on ex-service high pressure blade TBCs, *Surf. Coat. Technol.* 208 (2012) 39–45.
- [6] S. Kramer, J. Yang, C.A. Johnson, C.G. Levi, Thermochemical interaction of TBC with molten $CaO-MgO-Al_2O_3-SiO_2$, *J. Am. Ceram. Soc.* 89 (10) (2006) 3167–3175.
- [7] R. Wellman, G. Whitman, J.R. Nicholls, CMAS corrosion of EB-PVD TBCs: identifying the minimum level to initiate damage, *Int. J. Refract. Met. Hard Mater.* 28 (2010) 124–132.
- [8] A.K. Rai, R.S. Bhattacharya, D.E. Wolfe, T.J. Eden, CMAS-resistant thermal barrier coatings (TBC), *Int. J. Appl. Ceram. Technol.* 7 (2010) 662–674.
- [9] N. Chellah, Université de Lorraine, ONERA, Contribution à la compréhension de la dégradation chimique de barrière thermique en zircone yttrée par les CMAS en vue de proposer une nouvelle composition céramique résistante dans le système $ZrO_2-Nd_2O_3$, 2013, p. 235.
- [10] G. Pujol, Thèse, Université de Toulouse 3, DGA-SNECMA, Elaboration par voie sol-gel de nouvelles barrières thermiques architecturées présentant des propriétés contre l'infiltration des oxydes CMAS, étude de la réparabilité des systèmes endommagés, 2014, p. 173.
- [11] T. Ikegami, T. Mori, Y. Yajima, S. Takenouchi, T. Misawa, Y. Moriyoshi, Fabrication of transparent yttria ceramics through the synthesis of yttrium hydroxide at low temperature and doping by sulfate ions, *J. Ceram. Soc. Jpn.* 107 (3) (1999) 297–299.
- [12] D. Sordelet, M. Akinc, Preparation of spherical monosized Y_2O_3 precursor particles, *J. Colloid Interface Sci.* 122 (1988) 47–59.
- [13] T. Sato, S. Imaeda, K. Sato, Thermal transformation of yttrium hydroxides to yttrium oxides, *Thermochim. Acta* 133 (1988) 79–85.
- [14] A. Dupont, C. Parent, B.L. Garrec, J.M. Heintz, Size and morphology control of Y_2O_3 nanopowders via a sol-gel route, *J. Solid State Chem.* 171 (2003) 152–160.
- [15] J.M. Heintz, A. Dupont, C. Parent, B.L. Garrec, P. Guionneau, J. Etourneau, Grain morphology memory: yttria as study case, *Key Eng. Mater.* 264–268 (2004) 15–20.
- [16] M.P. Borom, C.A. Johnson, L.A. Peluso, Role of environment deposits and operating surface temperature in spallation of air plasma sprayed thermal barrier coatings, *Surf. Coat. Technol.* 86–87 (1996) 116–126 (PART 1).
- [17] L. Piaggi Ravaro, L. Vicente de Andrade Scalvi, Influence of pH of colloidal suspension on the electrical conductivity of SnO_2 thin films deposited via sol-gel dip-coating, *Mater. Res.* 14 (1) (2011) 113–117.
- [18] J. Zhu, W. Li, M. Zhu, W. Zhang, W. Niu, G. Liu, Influence of the pH value of a colloidal gold solution on the adsorption spectra of an LSPR assisted sensor, *AIP Adv.* 4 (2014) 031338-6.
- [19] S.D. Han, S.Y. Huang, G. Campet, M.A. Kennard, Y.M. Son, Influence of the pH values of the sol-gel state on the properties of SnO_2 powders obtained from a sol-gel route, *Act. Passiv. Electron. Comp.* 18 (1995) 53–60.
- [20] M. Kahlweit, Ostwald ripening of precipitates, *Adv. Colloid Interface Sci.* 5 (1975) 1–35.
- [21] W.D. Kingery, M. Berg, Study of the initial stages of sintering solids by viscous flow, evaporation-condensation, and self-diffusion, *J. Appl. Phys.* 26 (1955) 1205–1210.
- [22] R. David, P. Marchal, B. Marcant, Modeling of agglomeration in industrial crystallization from solution, *Chem. Eng. Technol.* 18 (1995) 1–8.
- [23] T.E. Hsieh, R.W. Balluffi, Experimental study of grain boundary melting in aluminium, *Acta Mater.* 37 (1989) 1637–1644.